

Synthesis and characterization of CuO nanoparticles using strong base electrolyte through electrochemical discharge process

PURUSHOTTAM KUMAR SINGH¹, PANKAJ KUMAR¹, MANOWAR HUSSAIN¹,
ALOK KUMAR DAS^{1,*} and GANESH CHANDRA NAYAK²

¹Department of Mechanical Engineering, Indian School of Mines, Dhanbad 826 004, Jharkhand, India

²Department of Applied Chemistry, Indian School of Mines, Dhanbad 826 004, Jharkhand, India

MS received 21 August 2015; accepted 19 October 2015

Abstract. In the present study, cupric oxide (CuO) nanoparticles were synthesized by electrochemical discharge process using strong base electrolytes. The experiments were carried out separately using NaOH and KOH electrolytes. The mass output rate and the crystal size were obtained with variation of the rotation speed of magnetic stirrer for both types of electrolytes. The mass output rate of CuO nanoparticles increased with the increase in the speed of rotation, and, after an optimum speed, it started decreasing. However, the size of the particles reduced with the increase of the rotation speed. The crystal plane of the obtained CuO nanoparticles was similar for both the electrolytes whereas the yield of nanoparticles was higher in KOH as compared with NaOH under the same experiment conditions. In this set of experiments, the maximum output rates obtained were 21.66 mg h⁻¹ for NaOH and 24.66 mg h⁻¹ for KOH at 200 rpm for a single discharge arrangement. The average crystal size of CuO particles obtained was in the range of 13–18 nm for KOH electrolyte and 15–20 nm for NaOH electrolyte. Scanning electron microscopy images revealed that flower-like and caddice clew-shaped CuO nanocrystalline particles were synthesized by the electrochemical discharge process. Fourier transform infrared spectrum showed that the CuO nanoparticles have a pure and monolithic phase. UV-vis-NIR spectroscopy was used to monitor oxidation course of Cu→CuO and the band gap energy was measured as 2 and 2.6 eV for CuO nanoparticle synthesized in NaOH and KOH solutions, respectively.

Keywords. Electrochemical discharge; CuO; nanoparticles; strong base.

1. Introduction

Nanoparticles are the most fundamental components in the fabrication of a nanostructure. Novel properties of nanoparticles are gaining increasing attention of the researchers. They are considerably smaller than the everyday objects around us that are governed by Newton's laws of motion. However, they are bigger than an atom or a simple molecule that are subjects of quantum mechanics [1]. In general, the size of a nanoparticles varies within the range of 1–100 nm. They are classified into three types on the basis of their dimension, i.e., one-, two- and three-dimensional-nanoparticles [2].

One-dimensional nanoparticles, such as, thin film, has been used for decades in the field of electronics, chemistry and engineering. Nowadays, they are used in solar cells, information storage system, chemical and biological sensors, magneto-optic and fibre-optic systems. Two-dimensional nanoparticles mainly consist of nanotubes which are available in two forms: single-wall nanotubes and multi-wall nanotubes. Two-dimensional nanoparticles have larger remnant of magnetization properties [3]. α -Fe₂O₃ thin film [4] is the example of one-dimensional thin films and carbon nanotubes

[5], graphite nanotubes [6] and TiO₂ nanotubes [7] are appropriate examples of two-dimensional nanotubes. Three-dimensional nanoparticles are important for the nanometre-scale devices in the fields of science and engineering. They have the property of high catalytic activities [8].

Nanostructured transition metal oxides are a special group of nanomaterial, used in the development of numerous novel and smart materials. These transition metal oxide nanocrystals are much under focus due to their unique physical and chemical properties [9–23]. These properties are particularly dependent on the shape, size, composition and structures of the nanocrystals. With the reduction in particle size to the range of nanometres, there is a rise in their surface-to-volume ratio [24,25].

Nowadays, research work is under way on cupric oxide (CuO) nanoparticles due to their p-type semiconducting properties with a narrow band gap, monoclinic structure and giant magnetic field resistance [26–29]. CuO crystal structure possesses useful photovoltaic and photo-conductive properties due to its narrow band gap [30]. Large surface-to-volume ratio and the advantage of size ensure better physical and chemical properties in CuO nanoparticles in comparison to micro- or bulk particles. It comes under the category of transition metal oxide [31]. These metal oxide nanoparticles

* Author for correspondence (eralok@yahoo.co.in)

have been widely studied because of their promising applications in various fields of engineering, such as, gas sensors [32,33], bio-sensors [34–38], photo detector [39], energetic materials [40], magnetic storage media [41], super capacitors [42] and photo catalysis [43]. They are also used in biomedicine [44], where they act as heterogeneous catalysts facilitating conversion of hydrocarbons to carbon dioxide. They also enhance viscosity and thermal conductivity of nanofluids. Several processes have been used for synthesis of cupric oxide nanoparticles, which include sonochemical reduction [45–54], electron beam irradiation [55], solution combustion [56–60], reverse micelles [61], microwave irradiation [62,63], laser ablation [64,65], hydrothermal [66,67], flame spray pyrolysis [68] and arc discharge process [69–72]. It is, however, a challenge for a material scientist to synthesize material oxide nanoparticles with controlled size and morphology as well as highest purity by means of a cost-effective technique.

In the present study, an electrochemical discharge method [73–75] (with basic electrolyte solution) has been used for synthesis of cupric oxide nanoparticles. NaOH and KOH electrolytes were used in the process. However, to ensure good in oxidizability, no surfactants were used in the process.

2. Experimentation and characterization processes

2.1 Materials

Sodium hydroxide pellets and potassium hydroxide pellets with 99.9% purity and produced by Merck and ethylalcohol from Yangyuan Chemical, China, with 99.9% purity were used. Distilled water was used to prepare strong electrolyte. A polished copper cathode (1-mm diameter) and an anode (4 cm × 4 cm) were used for the synthesis of CuO nanoparticles.

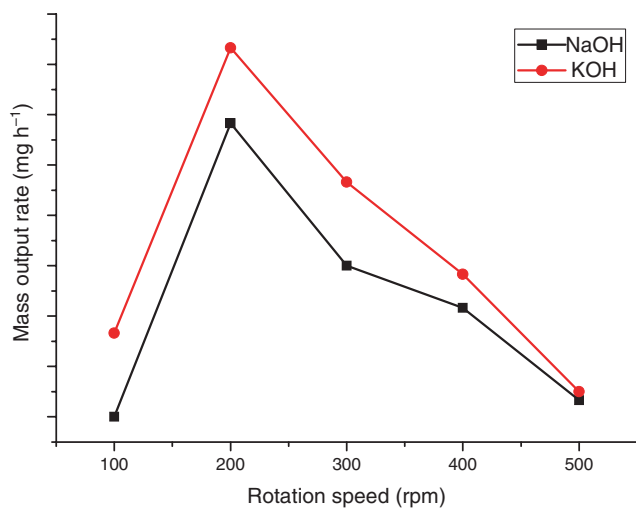


Figure 1. Effect of stirrer rotation speed on mass output rate of CuO nanoparticles.

2.2 Experiment preparation

High purity (cat. 98%) copper wire (1-mm diameter) and copper sheet (4 cm × 4 cm) were used as the electrodes. One of the copper electrodes (anode) was dipped into alkaline solution. The end of the other copper electrode (cathode) was momentarily brought into contact with the surface of the alkaline solution. When a threshold voltage was applied across the electrodes from a direct current supply, arc discharge could be observed at the cathode surface. During the experiment, 85 V was applied to the electrodes.

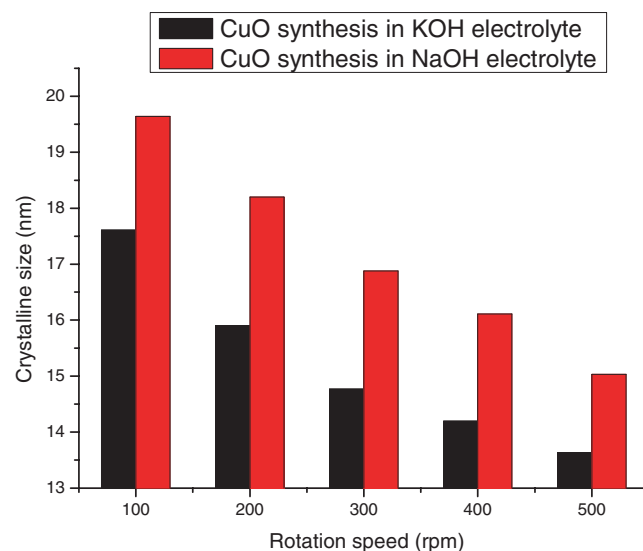


Figure 2. Effect rotation speed of electrolyte on crystalline size of CuO nanoparticles.

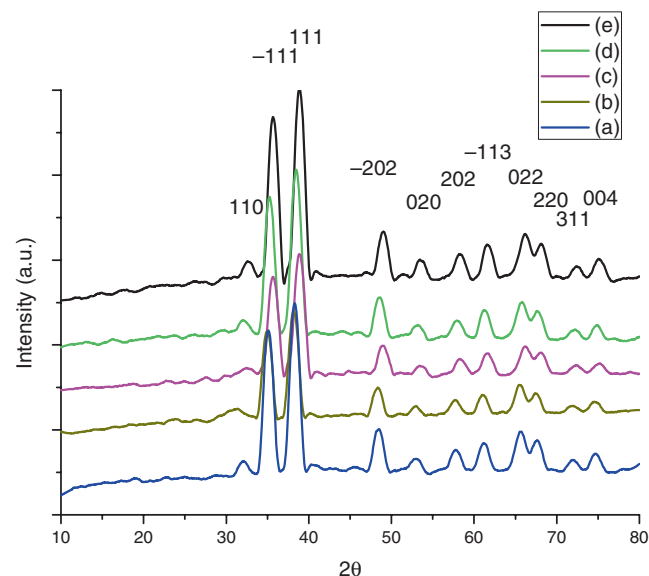


Figure 3. XRD patterns of CuO nanoparticles prepared in KOH electrolyte via electrochemical discharge process at different stirrer rotation speeds: (a) 100; (b) 200; (c) 300; (d) 400; and (e) 500 rpm.

Due to the discharge, the surface material is heated beyond its melting point, and, hence, the molten copper metal is dispersed into the solution. The sudden cooling of the molten metal droplets leads to the formation of nano-size particles. During the experiment, the nanoparticle-mixed electrolyte was centrifuged at 10,000 rpm. As a result, the particles were settled at the bottom of the test tubes as black precipitates. The black precipitates were washed with distilled water and ethyl alcohol for about six to seven times by the process

of centrifuging and finally was dried in an oven at 65°C for 8 h.

2.3 Characterization of produced particles

2.3a X-ray diffraction (XRD) analysis: The X-ray data were recorded in terms of the diffracted X-ray intensities (I) vs. 2θ . The crystalline size was calculated with the help of Scherrer's formula, which is given as [76]

$$D = \frac{0.9\lambda}{\beta \cos \theta}, \quad (1)$$

where D is the crystallite size, β the full-width at half-maximum (FWHM) of the most intense diffraction peak in radians, θ the diffraction angle and λ the wavelength of X-ray radiation.

2.3b UV-vis-NIR spectroscopy: Several methods can be applied to characterize the optical properties and to obtain the band gap. UV-vis-NIR spectroscopy is one of the methods for determining the band gap of CuO nanoparticles. It is used for evaluating the optical absorption characteristic of CuO nanoparticles. Tauc's formula is used for determining the band gap of nanoparticles/nanomaterial, which is given in [76]

$$(\alpha h\nu)^n = c(h\nu - E_g), \quad (2)$$

where E_g is the absorption band gap, α the absorption coefficient, $h\nu$ the photoenergy, C the constant relative to the

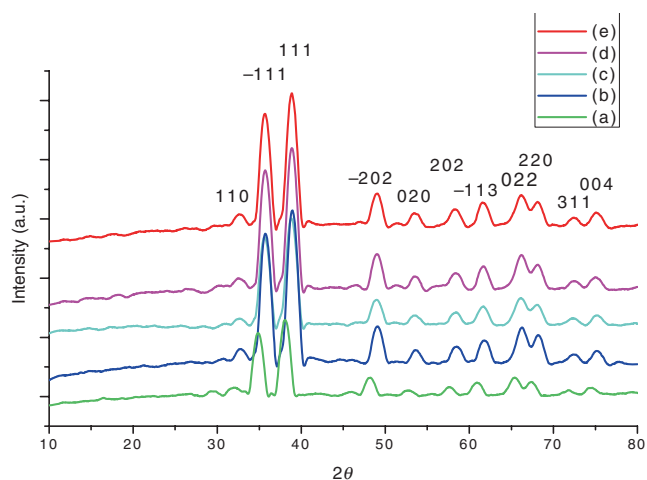


Figure 4. XRD patterns of CuO nanoparticles prepared in NaOH electrolyte via electrochemical discharge process at different stirrer rotation speeds: (a) 100; (b) 200; (c) 300; (d) 400 and (e) 500 rpm.

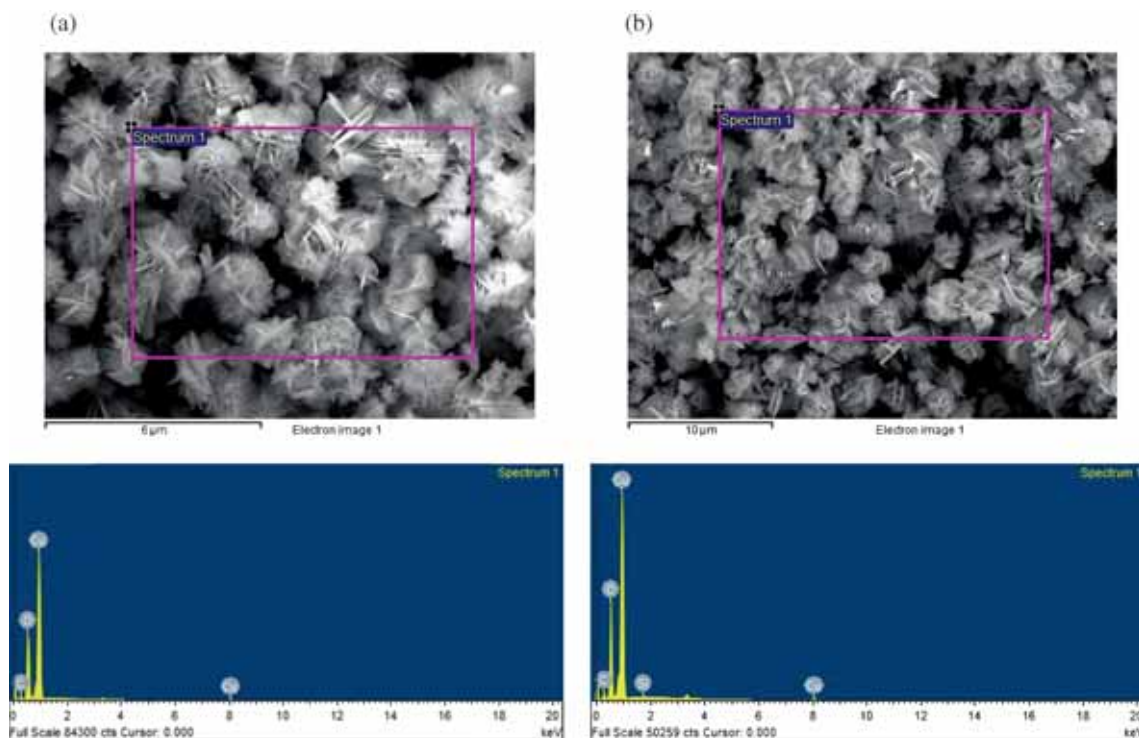


Figure 5. EDAX analysis of CuO synthesis in (a) KOH and (b) NaOH electrolytes.

material, and $n = 2$ for direct transition and $1/2$ for an indirect transition.

2.3c Fourier transform infrared (FTIR) spectrometry: The synthesized sample was analysed with FTIR spectrometry. During this process, a small amount of powder was mixed along with IR grade powder and then this powder was transferred into a sample cup of the diffuse reflectance accessory and scanned in a region of about $4000\text{--}500\text{ cm}^{-1}$.

2.3d Thermal gravimetric analysis/differential temperature analysis (TGA/DTA): TGA is a process which relies on measuring the change in physical and the chemical properties of a sample as a function of temperature (with constant heating rate) or as a function of time (with constant temperature). It is predominantly used for determining the features of a material that exhibit either mass loss or gain due to decomposition, oxidation or loss of volatiles.

DTA is a technique which rests on obtaining chemical composition of a substance under heating condition.

2.4 Morphological studies of nanoparticles

Morphology of the produced powder was analysed with field emission scanning electron microscopy (FE-SEM), model: Supra 55, Germany, which is equipped with energy-dispersive X-ray (EDX) system. The sample was kept on a sample stub with carbon tape. The stubs were placed in the sample chamber of FE-SEM. The accelerating voltage for FE-SEM examination was 5 kV.

3. Result and discussion

3.1 Effect of different electrolytes on CuO particles

In the synthesis process, the particle size, its phase, morphology, crystal structure and mass output rate depend on the type of electrolyte solution. Mass output rate, structure and size of particles vary with different electrolytes. In the present electrochemical discharge process, NaOH and KOH were used

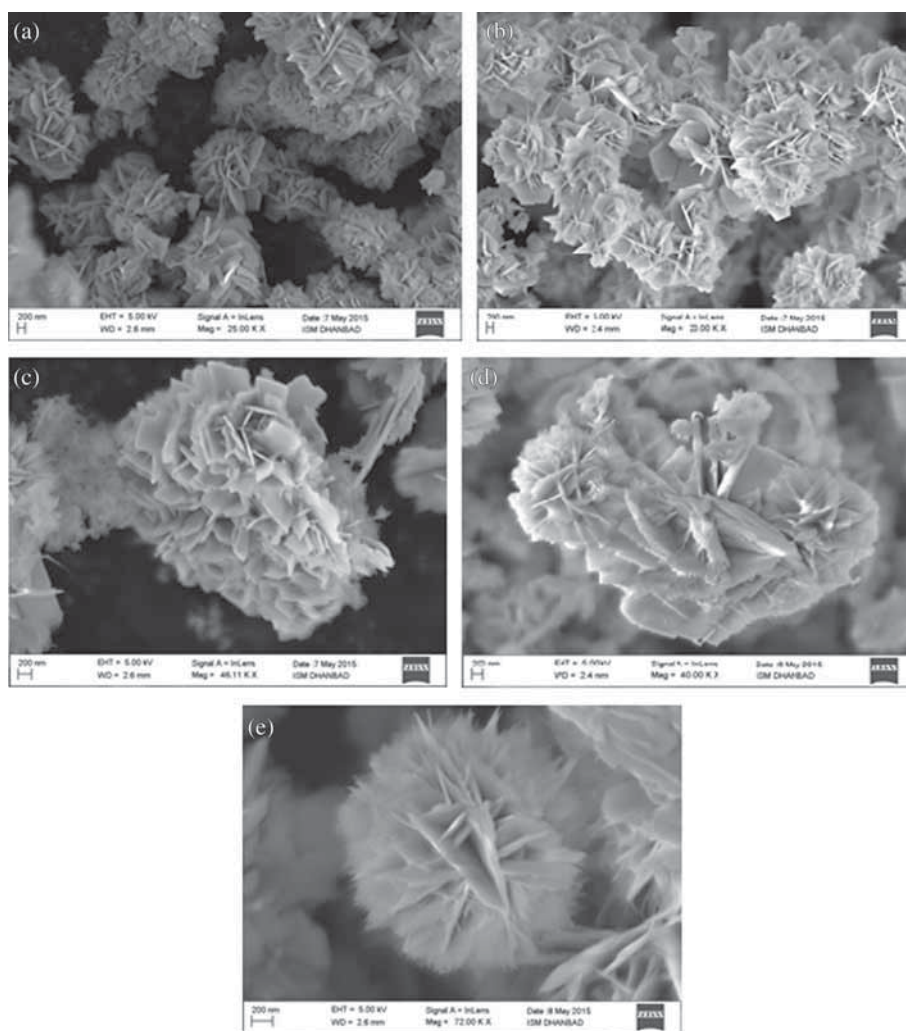


Figure 6. FE-SEM images of CuO prepared with KOH electrolyte at different stirrer speeds: (a) 100; (b) 200; (c) 300; (d) 400 and (e) 500 rpm.

as the electrolyte for synthesis of CuO nanoparticles. Higher mass output rate was obtained with KOH as compared to NaOH. So far, two kinds of explanation have been put forward on higher mass output rate, obtained in KOH. These interpretations are:

- (i) KOH electrolyte has lower viscosity than NaOH electrolyte [77], resulting in better flushing around the sparking zone in electrochemical discharge process. This facilitates better metal removal rate.
- (ii) The mobility and conductivity of K^+ ion is higher than Na^+ ion [78], leading to high conductivity of KOH electrolyte. As a result, more hydrogen bubbles are generated in KOH electrolyte solution. Hydrogen bubbles play a key role in generation of sparks and metal removal in the electrochemical discharge process.

Flower-like morphology could be attained with both the electrolytes. However, with NaOH, a few caddice clew-like morphology could be attained as well.

3.2 Effect of stirrer rotation speed on CuO nanoparticles

The mass output rate and morphology of particles also depend on the speed of rotation of the stirrer in the electrolyte. In this section, the effects of rotation speed on mass output rate and the size of CuO particles have been analysed by keeping other variables, i.e., the concentration of NaOH and KOH solution as well as working temperature constant. The rotation speed of the stirrer varied within the range from 100–500 rpm. The variation of results is presented in figure 1, which indicates that the mass output rate increases with increase of rotation speed up to an optimum level. Thereafter, it decreases with an increase of rotation speed. The stirrer rotation has direct effect on the mass output rate. At low rpm, the nanoparticles that are produced during the electrochemical spark cannot be removed fully from the discharge spot. On the other hand, at higher rpm, the hydrogen gas layer, which is formed over the surface of the electrode, is ruptured and strength of the spark is reduced. Hence, at the optimum rpm of the stirrer, the mass output rate of the

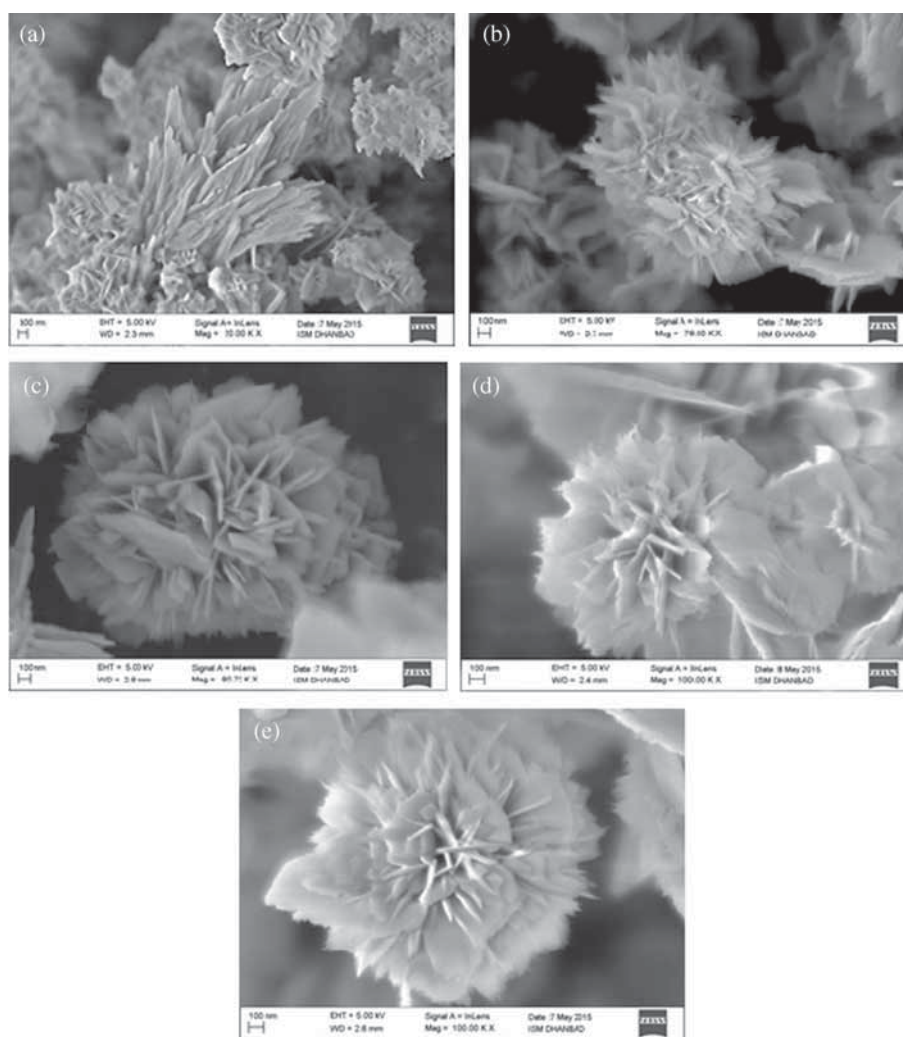


Figure 7. FE-SEM images of CuO prepared with NaOH electrolyte at different stirrer speeds: (a) 100; (b) 200; (c) 300; (d) 400 and (e) 500 rpm.

nanoparticles is higher. For the present parameter settings, the optimum rpm is 200.

In this set of experiments, for a single discharge arrangement, the maximum obtained output rates were 21.66 mg h^{-1} for NaOH and 24.66 mg h^{-1} for KOH at 200 rpm, respectively. The particle size of CuO was reduced with the increase of rotation speed. Figure 2 indicates the variation of particle sizes with the speed of rotation of the magnetic stirrer. With KOH electrolyte, smaller particle size could be realized as compared to NaOH.

3.3 Analysis of crystal structure

3.3a XRD: Figures 3 and 4 show the XRD pattern of the powder sample which was prepared at different rotation speeds through electrochemical discharge process. It was used for identifying the crystal size of CuO nanoparticles. The peaks in the XRD plots were sharp which indicated nanocrystalline structure. Bragg's reflection for CuO nanoparticles could be observed in XRD patterns at the diffraction peaks with 2θ angle value of 32.58, 35.53, 38.68, 48.93, 53.46, 58.18, 61.72, 66.26, 68.23, 72.56 and 75.12 corresponding to its crystal plane 110, $\bar{1}11$, 111,

$\bar{2}02$, 020, 202, $\bar{1}13$, 022, 220, 311 and 004, respectively. These crystal plane and reflection peak position values were nearly the same in both conditions of nanoparticle synthesis. However, with KOH electrolyte, the peaks were wider than NaOH electrolyte, which indicated that more residual stresses are induced in nanoparticles while produced with KOH. The differences in shape also suggested that the smaller sized CuO nanoparticles are synthesized in KOH electrolyte.

The crystal size of CuO particles can be obtained by using Scherrer's formula. The average crystal size of CuO particles that can be obtained is in the range of 13–18 nm for KOH electrolyte and 15–20 nm for NaOH electrolyte. The crystal size decreases with an increase in rotation speed of electrolyte, which is shown in figure 2. The results of EDAX are shown in figure 5. They indicate the presence of copper (Cu) and oxygen (O) as elementary components.

3.4 Analysis of nanoparticles morphology

3.4a SEM analysis: Figures 6 and 7 represent the FE-SEM images of nanoparticles which was prepared with

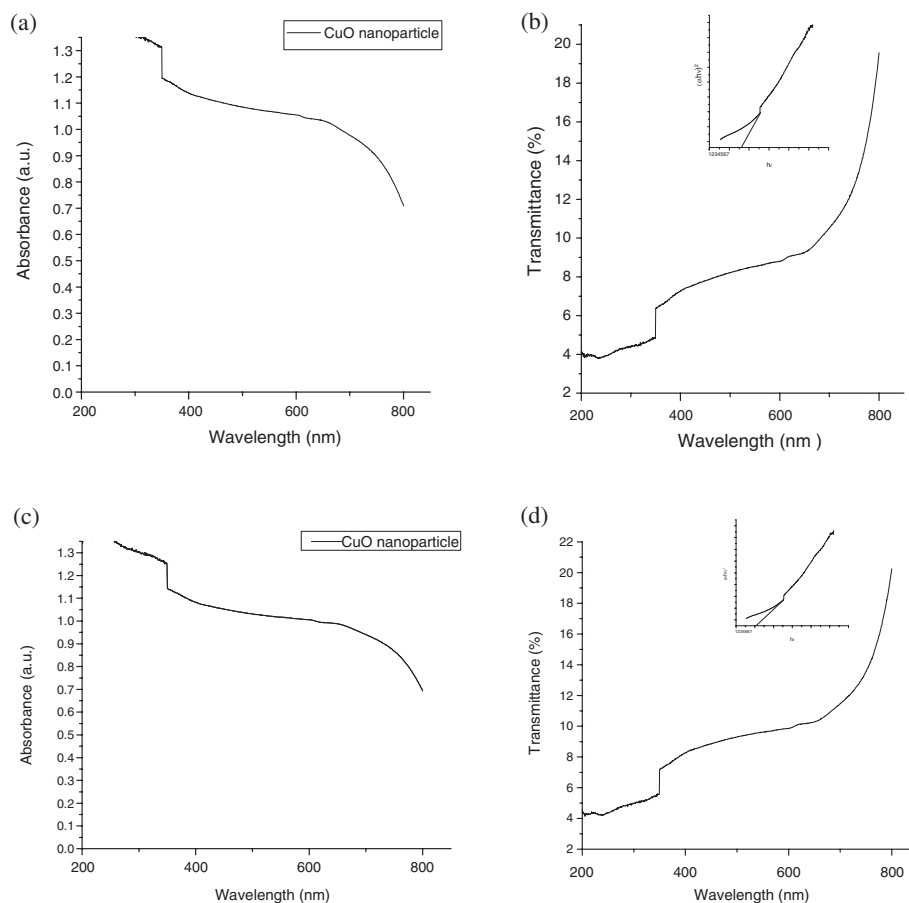


Figure 8. UV-vis-NIR absorption and transmittance spectra of CuO nanoparticles synthesized in (a, b) KOH and (c, d) NaOH electrolytes, respectively. The inset shows $(\alpha h\nu)^2 - h\nu$ curve.

KOH and NaOH electrolytes and with different rotation speeds of the magnetic stirrer. It was observed that a smaller particle size can be obtained with the KOH solution and at a higher rotation speed. The distributions of particles were satisfactory without any agglomeration effects. Flower- and caddice clew-type shapes could also be attained with the KOH solution. There was a sustainable change in the shape and size with variation of the rotation speed. This proposition holds good for KOH electrolyte. However, in case of NaOH electrolyte, except for a single structure (as shown in figure 7a), where CuO particles resembled caddice clew, the rest of the structures assumed a flower shape.

3.5 Optical characterization

3.5a UV-vis-NIR spectroscopy: UV-vis-NIR spectroscopy was used to estimate the direct band gap of CuO nanoparticles sample. The scan distance range was set between 200 and 800 nm. The absorbance vs. wavelength plots were converted to Tauc plot and band gap energy was calculated with the help of Tauc's formula. Tauc plot draws between $(\alpha h\nu)^2$ and $h\nu$. Its slope represents band gap energies of CuO nanoparticles. The band gap of the particles, produced in KOH and NaOH electrolyte, were 2.6 and 2 eV, respectively, which are larger than that of bulk CuO particles [79]. The band gap increases with the reduction of its size due to the quantum confinement effect [80,81]. This effect, which is enhanced by the band gap with its decreasing size, follows the relations which have been formulated below [81]

$$E_g = E_g(\infty) + \frac{h\pi}{2R^2} \left(\frac{1}{m_e} + \frac{1}{m_h} \right) - \frac{1.8e^2}{\epsilon R}, \quad (3)$$

where E_g is the effective band gap, $E_g(\infty)$ the bulk band gap, m_e and m_h the effect mass, h Planck's constant, R the radius of particles and ϵ the dielectric constant.

In small particles, they are confined to potential wells of small lateral dimension. It is the energy difference between the position of the conduction band and a free electron which leads to a quantization of their energy levels. These phenomena take place when the size of the particles becomes comparable to the de Broglie wavelength of a charge carrier. Therefore, in our present case, the particle size synthesized in KOH, is smaller than NaOH electrolyte. The optical absorption spectra and transmittance of CuO nanoparticles, synthesized in KOH and NaOH electrolytes, are shown in figure 8.

3.5b FTIR analysis: The infrared spectrums of synthesized samples of cupric oxide nanoparticles are shown in figure 9. This spectra of nano-sized CuO samples are presented in three regions. In the first region, the peaks observed in between 600 and 1050 cm^{-1} have strong absorption band. It is stretching of Cu-O along the $[-202]$ direction [82] due to the presence of CuO in monoclinic phase.

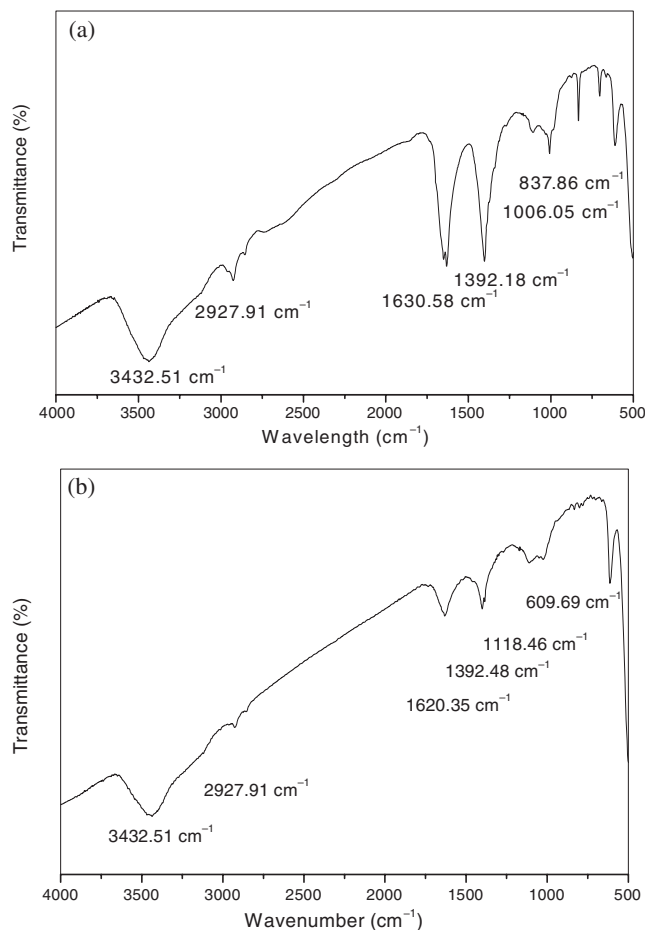


Figure 9. FTIR spectra of the CuO synthesized in (a) KOH and (b) NaOH electrolytes at 200 rpm stirrer speed.

In the second region (1350–1650 cm^{-1}), the peaks can be observed due to the presence of CO_2 in air. The third region starts from 2800 to 3500 cm^{-1} . Here, H_2O in the air and hydrated CuO samples are responsible for the creation of peaks. Therefore, it is confirmed through the FTIR spectrum results that synthesized CuO nanoparticles in KOH and NaOH electrolyte present pure and monolithic phase.

3.6 Thermal analysis

3.6a TGA/DTA: TGA of the CuO nanoparticle sample was carried out under a uniform heating rate of $10^\circ\text{C min}^{-1}$ and within the temperature range of 25–900°C. From figure 10, it can be ascertained that CuO sample undergoes minimum weight loss in both KOH and NaOH electrolyte. The weight loss is minimum because of the removal of residual H_2O and different gases. The chemical decomposition with an increase of temperature was examined through DTA and it appeared as the endothermic and exothermic peaks in the DTA curve. On the basis of both the prevailing conditions, the weight loss indicated dehydration of the sample. In other words, it meant loss of free and coordinated

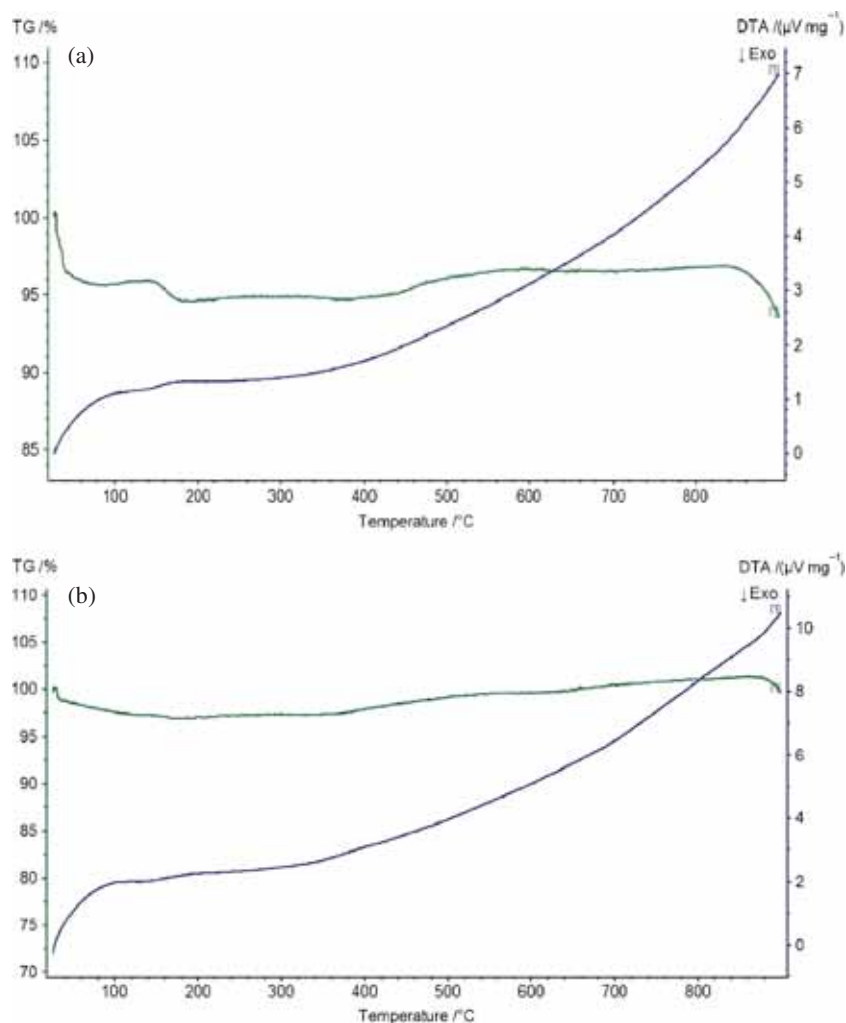


Figure 10. Thermal analysis of CuO nanoparticle synthesized in (a) KOH and (b) NaOH electrolytes.

water molecules up to 110°C from the sample. An initial weight loss of ~5% in KOH and ~3% in NaOH electrolyte was recorded. In KOH electrolytes, the weight loss could be recorded within the temperature range of 130–200°C. However, in NaOH electrolytes, no weight loss could be detected within this range. The result in the second stage was primarily consequent to the thermal decomposition noticed at around 820°C. Minor endothermic peaks could be observed with the DTA curve in the temperature range of 110–230°C under the previous conditions.

4. Conclusion

This study demonstrates that CuO nanoparticles having flower-like structure can be successfully developed through the electrochemical discharge method. The formation of CuO nanoparticles is influenced by different factors which include the rotation speed of electrolyte and the type of electrolyte solution. An increase in rotation speed of electrolyte

tends to promote the formation of smaller size nanoparticles. Also, mass output rate of nanoparticles increases with an increase of rotation speed up to an optimum level of 200 rpm. Thereafter, it reduces with the increase of rotation speed. Moreover, mass output rate, particle size and morphology of the nanoparticles are also influenced by the type of the electrolyte solution. In this study, higher mass output rate (24.66 mg h⁻¹) with small particle size was obtained in KOH compared to the NaOH electrolyte (21.66 mg h⁻¹). The band gap energy was measured as 2 and 2.6 eV for CuO nanoparticles, synthesized in NaOH and KOH solutions, respectively.

Acknowledgements

We would like to thank Dr G C Nayak from Applied Chemistry Department and Dr T K Mondal from Fuel and Mineral Engineering Department of ISM, Dhanbad, for extending their support for characterization of nanoparticles during this research work.

References

- [1] Horikoshi S and Serpone N (Eds) 2013 *Microwaves in Nanoparticle Synthesis: Fundamentals and Applications* (John Wiley & Sons)
- [2] Hett A 2004 *Nanotechnology: Small Matter, Many Unknowns* (Zurich, Swiss Reinsurance Company)
- [3] Poddar P, Telem-Shafir T, Fried T and Markovich G 2002 *Phys. Rev. B* **66** 060403
- [4] Kumar P and Kumar R 2015 *Thin Solid Films* doi: 10.1016/j.tsf.2015.08.047
- [5] Edgeworth J P, Wilson N R and Macpherson J V 2007 *Small* **5** 860
- [6] Goupalov S V 2005 *Phys. Rev. B* **8** 085420
- [7] Bavykin D V, Gordeev S N, Moskalenko A V, Lapkin A A and Walsh F C 2005 *J. Phys. Chem. B* **18** 8565
- [8] Chen S, Duan J, Ran J, Jaroniec M and Qiao S Z 2013 *Energy Environ. Sci.* **6** 3693
- [9] Wang Z L 2004 *J. Phys.: Condens. Matter* **16** 829
- [10] Fernandez-Garcia M, Martinez-Arias A, Hanson J C and Rodriguez J A 2004 *Chem. Rev.* **104** 4063
- [11] Vayssieres L 2004 *Int. J. Nanotechnol.* **1** 1
- [12] Jun Y-W, Choi J-S and Cheon J 2006 *Angew. Chem. Int. Ed.* **45** 3414
- [13] Chen X and Mao S S 2007 *Chem. Rev.* **107** 2891
- [14] Laurent S, Forge D, Port M, Roch A, Robic C, Vander Elst L and Muller R N 2008 *Chem. Rev.* **108** 2064
- [15] Comini E, Baratto C, Faglia G, Ferroni M, Vomiero A and Sberveglieri G 2009 *Prog. Mater. Sci.* **54** 1
- [16] Dutta S, Chattopadhyay S, Sarkar A, Chakrabarti M, Sanyal D and Jana D 2009 *Prog. Mater. Sci.* **54** 89
- [17] Barth S, Hernandez-Ramirez F, Holmes J D and Romano-Rodriguez A 2010 *Prog. Mater. Sci.* **55** 563
- [18] Singh D P and Ali N 2010 *Sci. Adv. Mater.* **2** 295
- [19] Li Y and Somorjai G A 2010 *Nano Lett.* **10** 2289
- [20] Hu J, Chen M, Fang X and Wu L 2011 *Chem. Soc. Rev.* **40** 5472
- [21] Devan R S, Patil R A, Lin J-H and Ma Y-R 2012 *Adv. Funct. Mater.* **22** 3326
- [22] Tiwari J N, Tiwari R N and Kim K S 2012 *Prog. Mater. Sci.* **57** 724
- [23] Spencer M J 2012 *Prog. Mater. Sci.* **57** 437
- [24] Park J, Joo J, Kwon S G, Jang Y and Hyeon T 2007 *Angew. Chem. Int. Ed.* **46** 4630
- [25] Zheng H, Ou J Z, Strano M S, Kaner R B, Mitchell A and Kalantar-Zadeh K 2011 *Adv. Funct. Mater.* **21** 2175
- [26] MacDonald A H 2001 *Nature* **414** 409
- [27] Liu Y, Chu Y, Zhuo Y, Li M, Li L and Dong L 2007 *Cryst. Growth Des.* **7** 467
- [28] Vaseem M, Umar A, Kim S H and Hahn Y B 2008 *J. Phys. Chem. C* **112** 5729
- [29] Son D I, You C H and Kim T W 2009 *Appl. Surf. Sci.* **255** 8794
- [30] Xu J F, Ji W, Shen Z X, Tang S H, Ye X R, Jia D Z and Xin X Q 1999 *J. Solid State Chem.* **147** 516
- [31] Tran T H and Nguyen V T 2014 *Int. Sch. Res. Notices* 2014
- [32] Zhang J, Liu J, Peng Q, Wang X and Li Y 2006 *Chem. Mater.* **18** 867
- [33] Choi Y-H, Kim D-H, Han H S, Shin S, Hong S-H and Hong K S 2014 *Langmuir* **30** 700
- [34] Umar A, Rahman M M, Al-Hajry A and Hahn Y B 2009 *Electrochem. Commun.* **11** 278
- [35] Rahman M M, Ahammad A J, Jin J-H, Ahn S J and Lee J-J 2010 *Sensors* **10** 4855
- [36] Wang X, Hu C, Liu H, Du G, He X and Xi Y 2010 *Sens. Actuators B—Chem.* **144** 220
- [37] Hsu Y-W, Hsu T-K, Sun C-L, Nien Y-T, Pu N-W and Ger M-D 2012 *Electrochim. Acta* **82** 152
- [38] Huang J, Dong Z, Li Y, Li J, Wang J, Yang H, Li S, Guo S, Jin J and Li R 2013 *Sens. Actuators B—Chem.* **182** 618
- [39] Wang S B, Hsiao C H, Chang S J, Lam K T, Wen K H, Hung S C, Young S J and Huang B R 2011 *Sens. Actuators A—Phys.* **171** 207
- [40] Rossi C, Zhang K, Esteve D, Alphonse P, Tailhades P and Vahlas C 2007 *J. Microelectromech. Syst.* **16** 919
- [41] Dar M A, Kim Y S, Kim W B, Sohn J M and Shin H S 2008 *Appl. Surf. Sci.* **254** 7477
- [42] Zhang X, Shi W, Zhu J, Kharistal D J, Zhao W, Lalia B S, Hng H H and Yan Q 2011 *ACS Nano* **5** 2013
- [43] Liu J, Jin J, Deng Z, Huang S-Z, Hu Z-Y, Wang L, Wang C, Chen L-H, Li Y, Tendeloo G V and Su B L 2012 *J. Colloid Interface Sci.* **384** 1
- [44] Chang Y N, Zhang M, Xia L, Zhang J and Xing G 2012 *Materials* **5** 2850
- [45] Kumar R V, Diamant Y and Gedanken A 2000 *Chem. Mater.* **12** 2301
- [46] Vijaya Kumar R, Elgamiel R, Diamant Y, Gedanken A and Norwig J 2001 *Langmuir* **17** 1406
- [47] Ranjbar-Karimi R, Bazmandegan-Shamili A, Aslani A and Kaviani K 2010 *Physica B: Condens. Matter* **405** 3096
- [48] Singh I and Bedi R K 2011 *Solid State Sci.* **13**
- [49] Anandan S, Lee G J and Wu J J 2012 *Ultrason. Sonochem.* **19** 682
- [50] Eshed M, Lellouche J, Matalon S, Gedanken A and Banin E 2012 *Langmuir* **28** 12288
- [51] Shui A, Zhu W, Xu L, Qin D and Wang Y 2013 *Ceram. Int.* **39** 8715
- [52] Chen Y-J, Meng F-N, Yu H-L, Zhu C-L, Wang T-S, Gao P and Ouyang Q Y 2013 *Sens. Actuators B—Chem.* **176** 15
- [53] Yang X-D, Jiang L-L, Mao C-J, Niu H-L, Song J-M and Zhang S-Y 2014 *Mater. Lett.* **115** 121
- [54] Sonia S, Jayram N D, Kumar P S, Mangalaraj D, Ponpandian N and Viswanathan C 2014 *Superlattices Microstruct.* **66** 1
- [55] Qi X, Huang Y, Klapper M, Boey F, Huang W, Feyter S D, Müllen K and Zhang H 2010 *J. Phys. Chem. C* **114** 13465
- [56] Jadhav L D, Patil S P, Chavan A U, Jamale A P and Puri V R 2011 *Micro Nano Lett.* **6** 812
- [57] Bayansal F, Kahraman S, Çankaya G, Çetinkara H A, Güder H S and Çakmak H M 2011 *J. Alloys Compd.* **509** 2094
- [58] Umadevi M and Christy A J 2013 *Spectrochim. Acta Mol. Biomol. Spectrosc.* **109** 133
- [59] Christy A J, Nehru L C and Umadevi M 2013 *Powder Technol.* **235** 783
- [60] Naika H R, Lingaraju K, Manjunath K, Kumar D, Nagaraju G, Suresh D and Nagabhushana H 2015 *J. Taibah Univ. Sci.* **9** 7
- [61] Han D, Yang H, Zhu C and Wang F 2008 *Powder Technol.* **185** 286

- [62] Zhao Y, Zhu J J, Hong J M, Bian N and Chen H Y 2004 *Eur. J. Inorg. Chem.* **2004** 4072
- [63] Dagher S, Haik Y, Ayesha A I and Tit N 2014 *J. Lumin.* **151** 149
- [64] Khashan K S, Sulaiman G M and Abdulameer F A 2016 *Arab. J. Sci. Eng.* **41** 301
- [65] Jung H J, Yu Y and Choi M Y 2015 *Bull. Korean Chem. Soc.* **36** 3
- [66] Maul J, Brito A S, de Oliveira A L M, Lima S J G, Maurera M A M A, Keyson D, Souza A G and Santos I M G 2011 *J. Therm. Anal. Calorim.* **106** 519
- [67] Jiang T, Wang Y, Meng D, Wu X, Wang J and Chen J 2014 *Appl. Surf. Sci.* **311** 602
- [68] Chiang C-Y, Aroh K and Ehrman S H 2012 *Int. J. Hydrogen Energy* **37** 4871
- [69] Yao W-T, Yu S-H, Zhou Y, Jiang J, Wu Q-S, Zhang L and Jiang J 2005 *J. Phys. Chem. B* **109** 14011
- [70] Kassae M Z, Buazar F and Motamedi E 2010 *J. Nanomater.* **2010** 7
- [71] Karahaliou P K, Svarnas P, Georga S N, Xanthopoulos N I, Delaportas D, Krontiras C A and Alexandrou I 2012 *J. Nanopart. Res.* **14** 1
- [72] Goli M, Haratizadeh H and Abrishami M E 2014 *Ceram. Int.* **40** 16071
- [73] Lal A, Bleuler H and Wüthrich R 2008 *Electrochem. Commun.* **10** 488
- [74] Wüthrich R and Mandin P 2009 *Electrochim. Acta* **54** 4031
- [75] Allagui A and Wüthrich R 2011 *Electrochim. Acta* **58** 12
- [76] Cullity B D and Stock S R 1978 *Principles of X-ray Diffraction* (Reading: Addison-Wesley)
- [77] Wüthrich R and Ziki J D A 2014 *Micromachining Using Electrochemical Discharge Phenomenon: Fundamentals and Application of Spark Assisted Chemical Engraving* (William Andrew)
- [78] Cao X D, Kim B H and Chu C N 2009 *Precis. Eng.* **4** 459
- [79] Wang H, Xu J Z, Zhu J-J and Chen H-Y 2002 *J. Cryst. Growth* **244** 88
- [80] Rehman S, Mumtaz A and Hasanain S K 2011 *J. Nanopart. Res.* **13** 2497
- [81] Phoka S, Laokul P, Swatsitang E, Promarak V, Seraphin S and Maensiri S 2009 *Mater. Chem. Phys.* **1** 423
- [82] Mohamed R M, Harraz F A and Shawky A 2014 *Ceram. Int.* **40** 2127